Analysis of Three-Dimensional Maximum Likelihood Algorithm for Capsule Endoscopy Localization

Shen Li[†], Yishuang Geng[†] Jie He[◇†] and Kaveh Pahlavan[†]

[†]CWINS Laboratory, ECE department
Worcester Polytechnic Institute (WPI)
Wrocester, USA
{shenli, ygeng, kaveh}@wpi.edu

[◇]School of Computer & Communication Engineering
University of Science & Technology Beijing (USTB)
Beijing, China
hejie1983@gmail.com

***Abstract*— Wireless capsule endoscopy (WCE) has become a good therapeutic method for a period of time. It helps detect, exam and heal gastro-intestinal (GI) related diseases. In the Capsule endoscopy application, knowledge of capsule position inside human body is rather important because it enables doctors locate the tumor of bleeding inside GI track and prepare for further therapeutic operations. However, due to the harsh environment for in-body wireless channel, in-body localization remains difficult and erroneous. In this paper, an improved three dimensional maximum likelihood algorithm has been introduced based on received signal strength (RSS) localization technology. Human body mesh and GI track mesh are built as the environment of algorithm simulation. Algorithm performance has been evaluated by comparison with the Cramer-Row Lower Bound (CRLB) and ranging error of the algorithm varies from 25mm to 140mm. By analyzing the results, we conclude that the three dimensional maximum likelihood is heavily impacted by the distance between implant and base station and its performance can be further improved.**

Keywords-component; maximum likelihood; RSS; in-body localization; CRLB; capsule endoscopy

I. INTRODUCTION

Body Area Network (BAN) can be referred to as a network technology established inside, on the surface of or in the surrounding area of human body. With time going on, BAN soon gains a huge reputation among different fields such as medical service, sport, insurance, social security, entertainment and even military. In medical or biomedical application, BAN systems are generally defined as an implanted body area network which is often consist of several nano-size sensors implanted in human body or distributed on the surface of human body which are capable for short-range wireless communication and biomedical signal monitoring [1].

Wireless Capsule Endoscope (WCE) is one of the most shining applications of BAN in the medical and biomedical area due to the fact that more than 19 million people are estimated suffering from gastro-intestinal (GI) related diseases [2]. In order to prevent, detect and heal GI diseases, doctors need a technology that can help them examine the GI track. In the old days, examine equipment was a flexible rubber tube with cable in the middle, mini-camera and tiny light attached to an end and patients had to swallow the rubber tube to help collect images from GI track [3]. However, the discomfort of having a tube stuck in the throat for hours has been eliminated with the born of WCE because for WCE equipment, the mini-camera and lights are compressed in a capsule-size, patient-friendly, painless and swallowable device that communicates with exterior apparatus wirelessly.

Apart from the GI images, Therapeutic operations and follow-up interventions also highly rely on the knowledge of position and orientation of the capsule [4]. Consequently, Investigation of localization technology for in-body wireless devices becomes increasingly important. Since the performance of Time of Arrival (TOA) technology are limited by the inadequate bandwidth (402-405MHz) of Medical Implant Communication Services (MICS) band and the Angle of Arrival (AOA) technology suffers from complexity and practical problem, Received Signal Strength (RSS) localization technology turns out to be the best choice for in-body localization [6,8]. In RSS based localization [6], the received signal strength of radio frequency wireless signal is measurable at the receiver side during the routine data communication without requiring additional power or occupying extra bandwidth [7]. Given the received signal strength and a proper path-loss channel model, the distance between transceivers can be easily calculated. Moreover, since a well-designed path-loss channel model has been already provided in the IEEE 802.15.6 draft for BAN standard, RSS based localization for in-body wireless device attacks more and more attention.

Due to the harsh environment of in-body wireless propagation channel, RSS based technology is notoriously unpredictable [6]. The strong absorption of in-body tissues and organs give raise to inconstancy of received signal strength, to make it worse, the slight motion of these tissues and organs aggravate the localization error. In order to limit the ranging error to the minimum, it is necessary to come up with accurate and efficient algorithms.

In this paper, an improved maximum likelihood algorithm is introduced and applied based on WCE application in the purpose of reducing ranging error and localization error during the in-body localization procedure. The scenario is that four base stations (BS) are evenly distributed on the front side of

This work is supported by the National Institute of Standards and Technology (Grand # 60NANB10D001)

human body and another four BSs mirroring on the back. The implant transmitter moves along the small intestine. Because of the shadow fading effect of in-body wireless channel, the ranging error of our algorithm ranges from 20mm to 145mm and the mean value of ranging error is 80mm. Software simulation result has been compared with general Cramer-Rao lower bound (CRLB) showing that the improved maximum likelihood algorithm has an excellent accuracy.

The remainder of this paper is organized as follow. Section II describes the scenario under which the algorithm simulation is conducted by measuring received signal strength between implant device and body surface attached base stations. In-body channel model and CRLB are also introduced. In section III, an improved maximum likelihood algorithm is reached based on the review of previous localization algorithms. Analysis of simulation results and comparison with CRLB are provided in section IV and section V concludes the paper.

II. SIMULATION ENVIRONMENT

A. Scenario

The localization system employed in this paper consist an implant transmitter and eight receivers. The transmitter goes along GI track and four receivers are evenly distributed on the lower part of the front side of abdomen, surrounding the stomach, small intestine and large intestine. The other four receivers are located on the back side, mirroring the front ones.

As is showed in figure 1, body muscle meshes and small intestine meshes share the same coordinate system, with the intestine meshes properly located inside human body. The muscle meshes used in simulation is in the size of *1800mm* x *600mm* x *400mm*, which generally fits various kinds of body type.

B. Channel model

The core of received signal strength based localization technology is the statistic path loss model for body area

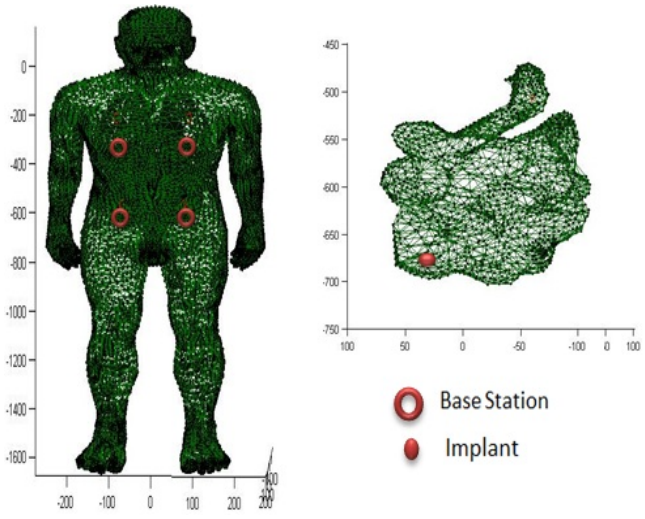

Fig. 1. Simulated body mesh, left is human body muscles with base station indicated by circles, right is small intestine with dot indicating the position of implant

Table 1.Parameters for the statistical implant to body surface path loss model[5].

Implant to body surface	$PL(d_0)$	n	σ_s
Deep Tissue	47.14	4.26	7.85
Near Surface	49.81	4.22	6.81

network. The complexity and continuously slight motion of human body make it difficult to come up with a static and accurate model. Consider that in free space, distance d between the transmitter and receiver determines the final path loss, implant to body surface model is given by combining path loss at reference distance d_0 and the effect of shadowing:

$$PL(d) = PL(d_0) + 10n\log_{10}(\frac{d}{d_0}) + S \quad (1)$$

$$S \sim N(0, \sigma_s),\ d_0 = 50mm \quad (2)$$

where $PL(d_0)$ represent the path loss at reference distance *50mm,* Coefficient n in the equation represent the path loss exponent, indicating the ratio between path loss increment and distance increment. Shadowing effect S follows a zero-mean normal distribution. The standard deviation σ_s reflects the path loss variation of the mean [5]. IEEE 802.15.6 committee partitions the implant to body surface channel to deep tissue scenario and near surface scenario. Since in the WCE application, capsule is located inside GI track, deep tissue scenario has been chosen in this paper, and the parameter values are listed in table 1. The whole model is developed at MICS band (402-405MHz).

C. Cramér–Rao Lower Bound

In estimation theory and statistics, the Cramér–Rao bound (CRB) or Cramér–Rao lower bound (CRLB) expresses a lower bound on the variance of estimators of a deterministic parameter. In its simplest form, the bound states that the variance of any unbiased estimator is at least as high as the inverse of the Fisher information.

The general form of Cramér–Rao lower bound can be obtained by considering an unbiased estimator $T(X)$ of a function $\psi(\theta)$ where θ is an unknown deterministic parameter of function $\psi(\theta)$, distributed according to specific probability density function $f(x, \theta)$. The unbiasness here can be understood as:

$$E\{T(X)\} = \psi(\theta) \quad (3)$$

in this case, the Cramér–Rao lower bound is given by:

$$\mathrm{var}(T) \geq \frac{[\psi'(\theta)]}{I(\theta)} \quad (4)$$

where $\psi'(\theta)$ is the derivative of $\psi(\theta)$, and $I(\theta)$ is the fisher information matrix. Apart from being a bound on estimators of functions of the parameter, this approach can be used to derive a bound on the variance of biased estimators with a given bias.

Consider an estimator $\hat{\theta}$ with bias $b(\theta) = E\{\hat{\theta}\} - \theta$ and let $\psi(\theta) = b(\theta) + \theta$, any unbiased estimator whose expectation is

$\psi(\theta)$ has variance greater than or equal to $(\psi'(\theta))2/I(\theta)$. Therefore any estimator $\hat{\theta}$ with bias $b(\theta)$ can be defined as:

$$\mathrm{var}(\hat{\theta}) \geq \frac{[1+b'(\theta)]^2}{I(\theta)} \tag{5}$$

and based on equation (5), mean squared error of biased estimator is bounded by:

$$E((\tilde{\theta}-\theta)^2) \geq \frac{[1+b'(\theta)]^2}{I(\theta)} + b(\theta)^2 \tag{6}$$

III. Maximum Likelihood Algorithm

A. Algorithm principle

Typical localization algorithms include Least-square, CN-TOAG, Nano and etc. [9-12]. Among these empirical algorithms, maximum likelihood centroid algorithm shows superior accuracy and can be used to estimate ranging error interval in real time. Most of empirical researches implement maximum likelihood algorithm in a two dimension indoor environment.

In localization area L, coordinate of n^{th} base station is defined as (x_n, y_n, z_n) and estimated distance between tag and n^{th} base station are defined as $\hat{d}_n$. (x, y, z) represent the position of tag and d_n represent the actual distance between tag and n^{th} base station. Ranging error ε_n can be given as:

$$\varepsilon_n = \hat{d}_n - d \tag{7}$$

and the ranging error interval caused by shadow fading is given as $M_n=[a_n, b_n]$, deriving the maximum and minimum estimated distance as:

$$D_{\max} = \hat{d} - a \tag{8a}$$

$$D_{\min} = \hat{d} - b \tag{8b}$$

The localization area L can be divided into three regions as is showed in figure 2.

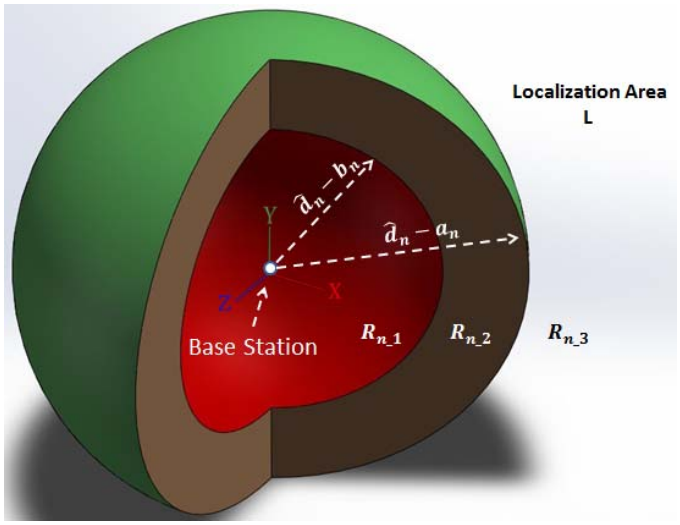

Fig. 2. Area divition for maximum likelihood algorithm

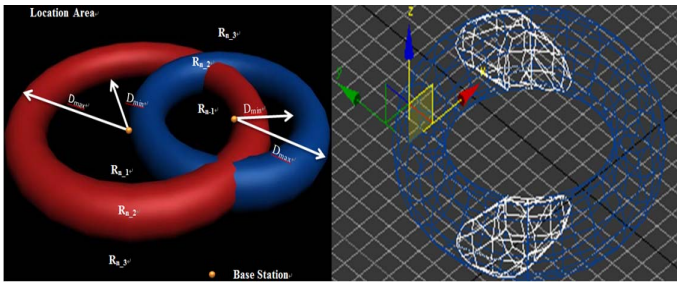

Fig. 3. (a) Maximum likelihood ranging area division. (b) bound of where the possible source reside.

- R_{n_1}: interior region, sector region centered at base station position (x_n, y_n, z_n) with a radius of D_{min}
- R_{n_2}: ring region, sector-ring region centered at base station position (x_n, y_n, z_n) with inner radius of D_{min} and outer radius of D_{max}
- R_{n_3}: exterior region, remained region in localization area L excluding R_{n_1} and R_{n_2}

Figure 3a shows the three dimensional regions in the algorithm considering two base stations and figure 3b illustrate the intersection area in a 3D coordinate system. Error interval for WCE application has been calculated by equation (1, 2) and the cumulative probability function (CDF) has been depicted in figure 4. From the CDF, the ring region for WCE application is worked out to be [-13dB, 13dB], dropping 5% erroneous localization results.

According to equation (1, 2) and the CDF in figure 4, the probability that implant is actually located in each region can be given as:

$$\begin{cases} P\{(x,y,z) \in R_{n\_1}\} \leq 5\% \\ P\{(x,y,z) \in R_{n\_2}\} \geq 90\% \\ P\{(x,y,z) \in R_{n\_3}\} \leq 5\% \end{cases} \tag{9}$$

Weight for each region can be defined as:

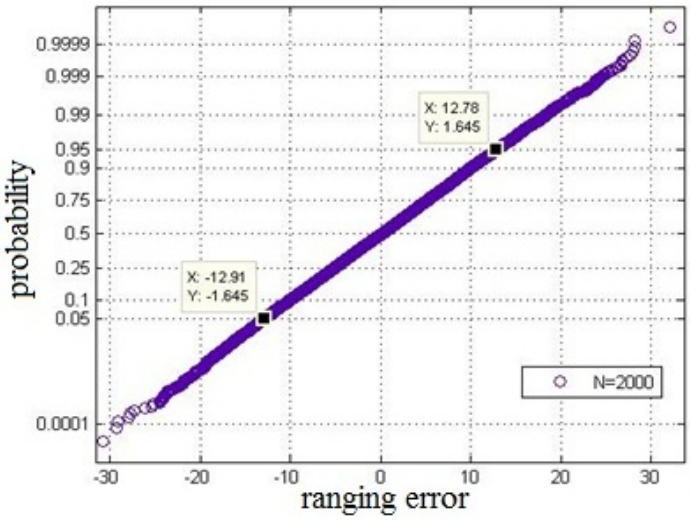

Fig. 4. Cumulative probability function of random Gaussian fading added in path loss

$$w_{n\_i} = \begin{cases} 1, i = 1 \ (for\ region\ R_{n\_1}) \\ 2, i = 2 \ (for\ region\ R_{n\_2}) \\ 1, i = 3 \ (for\ region\ R_{n\_3}) \end{cases} \quad (10)$$

For any region L_o is the intersection area of R_{n_a} and R_{n_b}, the region weight w_o should be the product of w_{n_a} and w_{n_b}.

B. Three Dimension Maximum Likelihood Algorithm

For the WCE application, assume that m BSs has been deployed to form the RSS based localization system together with the implant capsule. In this case, maximum likelihood algorithm can be estimated as follow.

Assume that implant communicates with each of the eight BSs and gets the RSS reading, thus the localization area L can be partitioned into:

- m interior regions: $R_{1\_1}, R_{2\_1}, \ldots, R_{m\_1}$
- m ring regions: $R_{1\_2}, R_{2\_2}, \ldots, R_{m\_2}$
- m exterior regions: $R_{1\_3}, R_{2\_3}, \ldots, R_{m\_3}$

After that, the intersection region can be given as:

$$L_o = R_{1\_1} \cap R_{1\_2} \cap \ldots \cap R_{1\_k} \cap R_{2\_1} \cap \ldots \cap R_{m\_k} \quad (11a)$$

$$w_o = w_{1\_1} \times w_{1\_2} \times \ldots w_{1\_k} \times w_{2\_1} \times \ldots \times w_{m\_k} \quad (11b)$$

$$m \in \{1,2,\ldots,8\}, k \in \{1,2,3\}, o \in \{1,2,\ldots,N\}$$

Finally, the region with largest weight is determined as the estimated region $L_{estimated}$ and the centroid of estimated region can be defined as the estimated position of implant:

$$(\hat{x}, \hat{y}, \hat{z}) = Centroid(L_{\max\ weight})$$

IV. Simulation Results

A. Comparison with Cramér–Rao Lower Bound

Cramer-Row Lower Bound is an important metric when evaluating and validating the accuracy and applicability of localization algorithms. Figure 5a shows a comparison between the CDF of the software simulation result and the CRLB. Observation tells that the result of CRLB performs much more static with a smaller variation range between 80mm and 110mm while the algorithm output ranging from 25mm to 140mm. However, even though the algorithm result and CRLB are different in ranging, their average output at cumulative probability of 0.6 confluences.

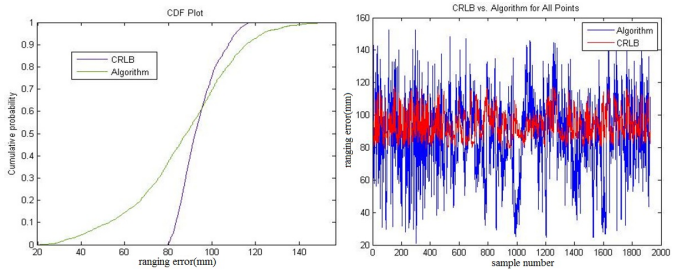

Fig. 5. (a) Comparison of CDF of Cramer-Rao lower bound against localization algorithm. (b) Point by point localization error of small intestine coordinates.

The localization errors of total 1926 coordinates in GI track are evaluated point by point in figure 5b. As can be seen from the figure, CRLB results in a gentle wave while the algorithm output suffers from severe fluctuations. This point by point plot again confirms the variation range difference between CDF of CRLB and algorithm result.

B. Minimum and Maximum Error Coordinate

To explain the difference between CDF and CRLB, the point with maximum and minimum localization error has been picked out (coordinate 316 for maximum localization error and coordinate 38 for minimum localization error).

In purpose of facilitating analysis, the intersection region of maximum and minimum point has been projected into the *YZ* plane and the thickness of human body *(X direction)* becomes temporarily invisible but its influence on the localization result still remains.

Simulation has been implemented for several times and two typical result of minimum error coordinate intersection region have been recorded in figure 6 and the result of maximum error coordinate intersection region is depicted in figure 7.

The minimum error coordinate has thinly scattered distribution and smaller intersection region ranging about 200mm in *Y* direction and 250 mm in *Z* direction. The maximum error coordinate always has a larger intersection region that ranges about 700mm in *Y* direction and 550mm in *Z* direction. Apart from that, during the simulation, minimum error coordinate and maximum coordinate always appear at a specific part of the small intestine mesh. As can be seen from figure 8a, the minimum error area is at the bottom right of human inner back while figure 8b shows that the maximum error area is in the core of human body.

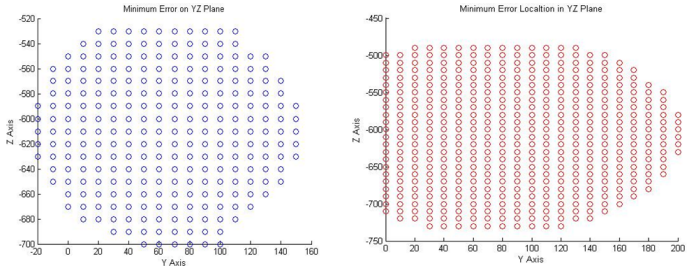

Fig. 6. Projection of intersection area for minimum error coordinate on *YZ* plane

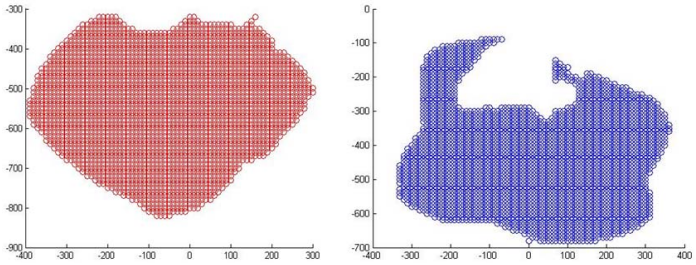

Fig. 7. Projection of intersection area for maximum error coordinate on *YZ* plane

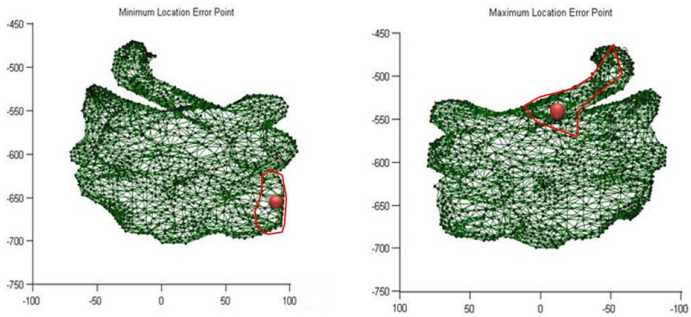

Fig. 8. (a)Minimum localization error coordinate area in small intestine. (b)Maximum localization error coordinate area in small intestine

C. *Analysis of Coordinate Position*

Figure 9 depicts the procedure of maximum likelihood algorithm at the minimum error coordinate. In figure 9a, eight base stations are deployed and the eight red circles indicate D_{max} while the eight green circles indicate the D_{min} on the *YZ* plane. Figure 9b is the zoom-in of figure 9a in which the D_{max} for the nearest base station can be observed in the center, limiting the estimated location area in a relatively small scale.

Similar to the minimum error case, figure 10 shows the scatter plot of maximum error coordinate intersection area. As can been seen from the figure, the intersection area of maximum error coordinate is much larger than that of minimum error coordinate. Reasons can be partitioned into two parts. First and foremost, the green circles representing D_{min} in figure 10b is larger than those green circles in figure 9b. Moreover, no minor red circle can be found in the middle of maximum error coordinate intersection area, thus unable to limit the localization error in a relatively small scale.

Based on the previous analysis, we conclude that in our three dimensional improved maximum likelihood algorithm, implant positions have strong impact on algorithm performance. When the implant is located close to any base station,

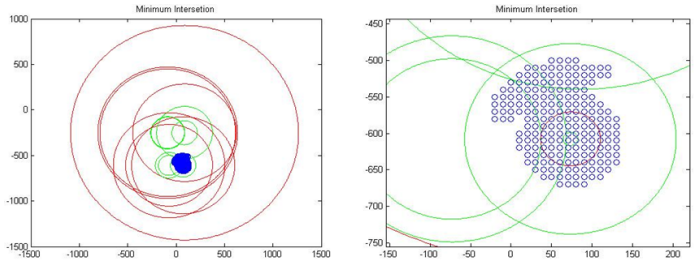

Fig. 9. Intersection area for minimum error coordinates

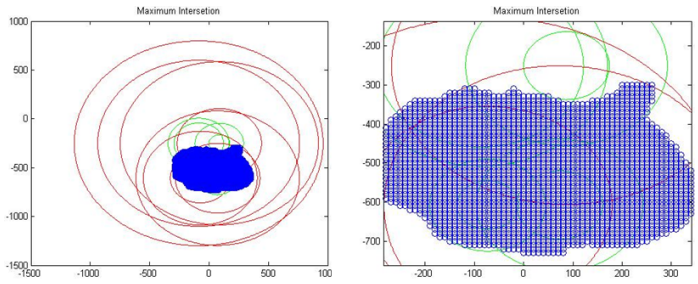

Fig. 10. Intersection area for maximum error coordinates

localization error turns out to be acceptable and the algorithm performance becomes good. Otherwise, when the implant is located in the middle of human body, the localization error raises because of being far away from base stations.

The algorithm performance is partially superior to Cramer-Row lower bound is mainly because in this paper, the Cramer-Row lower bound takes the whole human body into consideration. It is intuitive that by reducing the sample area, Cramer-Row lower bound will result in lower localization error.

V. CONCLUSION

In this paper, we introduced an improved three dimensional maximum likelihood algorithm for in-body capsule endoscopy localization and analyzed the algorithm performance. The algorithm is presented for RSS based localization and the ranging error varies from 25mm to 140mm, partially superior to the overall human body Cramer-Rao Lower Bound. To explain that, several more simulation has been conducted and we observe that the minimum error coordinates distribute near body surface, very close to one of the base station while the maximum error coordinates are located near the center of human body, relatively far away from all of the base stations. As a result, the location of implant has a strong impact on the performance of this RSS based localization algorithm.

REFERENCES

[1] Swar Pranay, “Accuracy of Localization System inside Human Body using a Fast FDTD Simulation Technique,” Medical Information and Communication Technology (ISMICT), 2012

[2] M. Yu, “M2A(TM) Capsule Endoscopy: A Breakthrough Diagnostic Tool for Small Intestine Imaging,” Gastroenterology Nursing, vol. 25, pp. 24-27, 2002.

[3] J. D. Mellinger “Upper Gastrointestinal Endoscopy: Current Status,” Surgical Innovation, vol. 10. Pp. 3-12, March 1, 2003.

[4] J. L. Toennies, G. Tortora, M. Simi, P. Valdastri and R. J. Webster, “Swallowable medical devices for diagnosis and surgery: The state of art,” Proceedings of the Institution of Mechanical Engineers, Part C: Journal of Mechanical Engineering Science, vol. 224, pp. 1397-1414, January 1, 2010.

[5] IEEE, 802.15 Tg6 ,“Draft of Channel Model for Body Area Network”, November, 2010.

[6] J. He, Y. Geng and K. Pahlavan, “Modeling TOA Ranging Error for Body Mounted Sensors, ” IEEE 23nd International Symposium on Personal, Indoor and Mobile Radio Communications, 2012, accepted.

[7] Swar Pranay, ”On Effect of Transmit Power Variance on Localization Accuracy in Wireless Capsule Endoscopy,” Wireless Commication and Networking Conference(WCNC), pp. 2119-2123, 2012

[8] Y. Ye, U. Khan, N. Alsindi, R. Fu and K. Pahlavan, “On the accuracy of RF positioning in multi-Capsule endoscopy,” IEEE 22nd International Symposium on Personal, Indoor and Mobile Radio Communications, 2011

[9] J. He, Q. Wang, Q. Zhang, B. Liu and Y. Yu, "A practical indoor TOA ranging error model for localization algorithm," IEEE 22nd International Symposium on Personal, Indoor and Mobile Radio Communications, 2011.

[10] M. Kanaan and K. Pahlavan, "A comparison of wireless geolocalization algorithms in the indoor environment", IEEE Wireless Communications and Networking Conference (WCNC 2004), Atlanta, GA, USA, 21-25 March 2004.

[11] Nanotron Corporation, "NanoLOC Development Kit 1.0 Factsheet".

[12] M. Kanaan and K. Pahlavan, "CN-TOAG: A new algorithm for indoor geolocaiton", 15th IEEE International Symposium on Personal, Indoor and Mobile Radio Communications (PIMRC), 2004.